Acta Cryst. (1984). C**40**, 335–340

Deformation Electron Density of Lithium Nitrate Trihydrate, $LiNO_3.3H_2O$, at 120 and 295K*

BY KERSTI HERMANSSON, JOHN O. THOMAS AND IVAR OLOVSSON

Institute of Chemistry, University of Uppsala, Box 531, *S*-751 21 *Uppsala, Sweden*

(*Received* 18 *February* 1983; *accepted* 18 *October* 1983)

Abstract. $M_r = 123{\cdot}00$, orthorhombic, *Cmcm*, $Z = 4$; at 120 K, $a = 6{\cdot}713\ (7)$, $b = 12{\cdot}669\ (4)$, $c = 5{\cdot}968\ (5)$ Å, $V = 507{\cdot}7\ (7)$ Å^3; at 295 K, $a = 6{\cdot}8018\ (4)$, $b = 12{\cdot}7132\ (9)$, $c = 5{\cdot}9990\ (4)$, $V = 518{\cdot}75\ (6)$ Å^3; m.p. = 303·1 K, $D_x = 1{\cdot}575$ g cm^{-3} (295 K), $F(000) = 256$; X-ray data (Mo $K\alpha$, $\lambda = 0{\cdot}71069$ Å) have been collected at 120 K; final $wR(F^2)$ values 0·064 from conventional spherical-atom refinement and 0·033 from deformation refinement. The deformation electron density of $LiNO_3.3H_2O$ has been studied at 120 K (new data) and 295 K in order to compare static and dynamic deformation maps derived at two temperatures. A combination of X-ray and neutron data has been used both for the *X–N* and the multipolar expansion maps. *Dynamic* density peaks in bonds and lone-pair regions are, in general, 0·10–0·20 e Å^{-3} lower at 295 than at 120 K. The agreement between the *static* deformation maps at the two temperatures is unsatisfactory (especially for the water molecules) due to the large number of weak reflections in the 295 K data set. This leads to large correlations in the 295 K refinements. The dynamic deformation density of the NO_3^- ion at 120 K shows lone-pair and bond-peak maxima of 0·20–0·40 e Å^{-3}. The N—O bond peaks are elongated perpendicular to the molecular plane. The water molecules show well developed deformation features and the hydrogen-bond density is consistent with what is usually observed for medium-strong hydrogen bonds.

Introduction. $LiNO_3.3H_2O$ has been chosen as one of a series of simple hydrates for which the deformation electron density is investigated by means of a combination of X-ray and neutron diffraction data. The valence-to-core ratio in $LiNO_3.3H_2O$ is high with an *S* value, defined as $V_{cell}/\sum_{cell} n^2_{core}$ (see Stevens & Coppens, 1976), of 4·0.

This paper presents an analysis of the electron density at 295 and 120 K by means of a multipolar expansion of the deformation density and the *X–N* technique. Four different data sets form the basis of the analysis. The experimental details relating to the 295 K X-ray data have been published by Hermansson, Thomas & Olovsson (1977); the structure solution was also presented in the same paper. The two neutron diffraction experiments at 120 and 295 K have been described by Hermansson, Thomas & Olovsson (1980). The first part of the present paper contains the experimental details for the X-ray 120 K data set. The deformation models used are then presented, followed by a discussion of the features of the deformation electron density at the two temperatures. A comparison of positional and thermal parameters obtained from the various data sets and using different refinement procedures is also given.

Experimental. Some experimental details for the X-ray data collection at 120 K are listed in Table 1. The corresponding information for the 295 K X-ray data set is also given for comparison.

Approximately spherical crystal, radius 0·085 mm; grown by evaporation from aqueous solution of $LiNO_3$; sealed in thin-walled glass capillary; graphite-monochromatized Mo $K\alpha$ radiation, continuous ω/θ scan; scan width in ω according to $\Delta\omega = (1{\cdot}00 + 0{\cdot}35 \tan\theta)°$, $\sin\theta/\lambda \leq 0{\cdot}94$ Å^{-1}. Low temperature obtained by a cooled nitrogen gas-flow. Temperature variation less than ±5 K observed between different

Table 1. *Some experimental details for the two X-ray data collections*

	120 K	295 K
Radiation	Mo $K\alpha$	Mo $K\alpha$
Diffractometer	Nonius, CAD-4	Stoe–Philips, four-circle
$(\sin\theta/\lambda)_{max}$ (Å^{-1})	0·94	0·81
No. of reflections measured	2036	1238
No. of unique reflections, all	889	661
No. of reflections with $F_o^2 > 2\sigma(F_o^2)$	607	375
No. of reflections with $F_o^2 > 3\sigma(F_o^2)$	577	329
Transmission (all reflections)	0·98	0·99
Extinction level ($F^2_{o,\,uncorr} = yF^2_{o,\,corr}$)	4 reflections with $y < 0{\cdot}97$	3 reflections with $y < 0{\cdot}97$
$wR(F^2)$ values* $[F_o^2 > 3\sigma(F_o^2)]$		
conventional refinement	0·064	0·055
high-order refinement	0·060	0·122
deformation refinement (*A*)	0·033	0·030
deformation refinement (*B*)	0·038	0·028

* $wR(F^2) = [\sum w(F_o^2 - F_c^2)^2/\sum wF_o^4]^{1/2}$.

* Hydrogen Bond Studies. CXLVII.

0108-2701/84/030335-06$01.50

orientations of the goniometer head. To reduce icing on the crystal, a flow of dry air was passed through the lead-glass box surrounding the diffractometer. A relative humidity of 15% was maintained within the box. For all forms, several (two, three or four) symmetry-related reflections were measured.

The five test reflections showed intensity variations less than 1% during the data collection. The reflection intensities were obtained by the peak profile analysis method of Lehmann & Larsen (1974). Analysis of the agreement between 785 pairs of $\bar{h}\bar{k}\bar{l}$, hkl reflections in a normal probability plot (Abrahams & Keve, 1974) gave a straight line with slope 1·06 and intercept 0·04. Symmetry-related reflections averaged; $R_{\rm int} = 0{\cdot}015$; 889 unique reflections; corrections for Lorentz, polarization and absorption (the latter being redundant, however, since $\mu_{\rm calc} = 0{\cdot}163$ mm^{-1} and the transmission factor is 0·978 for all reflections).

Different types of refinement were carried out for both the room- and the low-temperature data sets (see Table 1).

(i) *Conventional spherical-atom refinements.* The spherical-atom refinement of the 295 K data set has been described earlier. Below some details for the 120 K refinement are given. $\sum w(F_o^2 - F_c^2)^2$ minimized. Reflections assigned weights according to the formula $w^{-1} = \sigma_c^2(F_o^2) + k^2F_o^4$, with k fixed empirically at 0·03. Spherical-atom scattering factors used for H, Li^+, N and O and anomalous-dispersion corrections for N and O taken from *International Tables for X-ray Crystallography* (1974). In the last cycle of refinement, the following parameters were refined: one scale factor, one extinction parameter [isotropic type I extinction according to Becker & Coppens (1974)], positional and anisotropic thermal parameters for non-hydrogen atoms, positional and isotropic thermal parameters for H atoms; 39 parameters in all. As indicated in Table 1, the level of extinction in the data set was very low. The four reflections with $0{\cdot}93 < y < 0{\cdot}97$ were excluded from the refinement. The final $wR(F^2)$ values are listed in Table 1, the resulting positional parameters in Table 2, and distances and angles in Table 3.*

(ii) *High-order refinements.* Data cut-offs of 0·70 Å^{-1} at 120 K and 0·60 Å^{-1} at 295 K, leaving 457 and 374 high-order reflections, respectively. For the H atoms, positions fixed at the neutron values and isotropic thermal parameters set to 2·5 and 3·5 Å^2 at 120 and 295 K, respectively; 29 refined parameters in all.

(iii) *Deformation refinements; model A.* Positional and anisotropic thermal parameters for non-H atoms refined along with the deformation coefficients. H-atom parameters fixed at their neutron values (for the 120 K structure the neutron thermal parameters were multiplied by a factor 1·13; see later); 103 parameters refined for 120 K data, 63 for 295 K data (see later).

(iv) *Deformation refinements; model B.* Positional and thermal parameters fixed at their neutron values (multiplied by 1·13 at 120 K); 75 parameters refined.

In the deformation refinements, the *static* deformation of the electron density from free spherical Hartree–Fock atoms or ions was expressed as a set of multipolar functions on each atom following the formalism of Hirshfeld (1971). Gaussian radial functions were used almost exclusively (an exponential dependence was tested but found to show poor convergence). The deformation coefficients up to the octapolar level were refined for all atoms; 73 coefficients in all. The radial exponents were set to 3·0, 4·0, 5·0 and 6·0 Å^2 for Li, H, N and O, respectively. Due to large correlation it was not possible to refine the exponents along with the other parameters. All atoms in $LiNO_3.3H_2O$ lie on special positions. No extra symmetry constraints were imposed on the deformation model. Axial symmetry about the O—H bonds was assumed for the H atoms. The weights used in the deformation refinements were $w^{-1} = \sigma_c^2(F_o^2) + k^2F_o^4$, with k equal to 0·03 and 0·01 for the 120 and 295 K data sets, respectively. The computer programs used have been described by Lundgren (1982).

Model A was successful in describing the deformation density at 120 K. The decrease in R values compared to the spherical-atom refinement suggests a significant improvement to the model (see Table 1).

Table 2. *Atomic coordinates* ($\times 10^5$) *and equivalent isotropic thermal parameters (expressed as the average r.m.s. amplitude) for the* 120 K *X-ray data set*

The first line refers to the spherical-atom refinement, the second to the deformation refinement (model *A*).

		x	y	z	$\bar{U}$(Å)
	Li	0	0	0	0·128
					0·127
	N	0	21647 (6)	25000	0·120
			21650 (10)		0·119
	O(1)	0	16906 (4)	6769 (11)	0·143
			16903 (10)	6784 (30)	0·143
	O(2)	0	31658 (5)	25000	0·153
			31641 (13)		0·154
	O(3)	28956 (7)	47920 (4)	25000	0·119
		28942 (17)	47912 (10)		0·119
	O(4)	0	64028 (6)	25000	0·138
			64059 (16)		0·138
$H_2O(3)$	H(1)	22588 (219)	42816 (102)	25000	
		21347*	41467*		
	H(2)	21921 (214)	52888 (105)	25000	
		19196*	53582*		
$H_2O(4)$	H(3)	0	67574 (104)	13862 (259)	
			68587*	12146*	

*Neutron values, not refined.

* Lists of structure factors and thermal parameters for the spherical-atom and deformation refinements (model *A*) have been deposited with the British Library Lending Division as Supplementary Publication No. SUP 38929 (22 pp.). Copies may be obtained through The Executive Secretary, International Union of Crystallography, 5 Abbey Square, Chester CH1 2HU, England.

There are only spurious peaks left in the residual map after the deformation refinement; no feature is greater than 0·15 e Å^{-3}, while for the spherical-atom refinement the maximum peak density in the residual map is 0·40 e Å^{-3}.

Table 3. *Interatomic distances* (Å) *and angles* (°) *at* 120 K

The first row refers to the spherical-atom X-ray refinement, the second to the deformation refinement model *A* and the third to the neutron data.

(*a*) Li^+ ion

Li–O(3)	2·072 (1)	O(3)–Li–O(3′)	94·01 (8)
	2·072 (2)		93·97 (9)
	2·075 (1)		93·82 (2)
Li–O(1)	2·180 (1)	O(3)–Li–O(3″)	85·99 (8)
	2·179 (1)		86·03 (9)
	2·182 (1)		86·18 (8)
		O(3)–Li–O(1)	89·51 (2)
			89·52 (5)
			89·47 (2)
		O(3)–Li–O(1′)	90·49 (2)
			90·48 (5)
			90·53 (2)

(*b*) NO_3^- ion

N–O(1)	1·243 (1)	O(1)–N–O(1)	122·20 (9)
	1·242 (2)		122·09 (17)
	1·239 (1)		122·09 (7)
N–O(2)	1·268 (1)	O(1)–N–O(2)	118·90 (5)
	1·266 (2)		118·95 (9)
	1·260 (1)		118·45 (3)

(*c*) H_2O molecules

	O–H···O	O–H	O···O	H···O
$H_2O(3)$	O(3)–H(1)···O(2)	0·78 (1)	2·832 (2)	2·07 (1)
		0·963 (1)*	2·833 (2)	1·898 (2)*
		0·961 (1)	2·834 (2)	1·901 (2)
	O(3)–H(2)···O(4)	0·79 (1)	2·818 (2)	2·04 (1)
		0·972 (1)*	2·821 (2)	1·850 (2)*
		0·969 (1)	2·818 (2)	1·850 (1)
$H_2O(4)$	O(4)–H(3)···O(1)		3·072 (1)	2·32 (1)
			3·068 (2)	2·158 (2)*
		0·80 (1)	3·069 (1)	2·157 (1)
		0·958 (2)*		
	O(4)–H(3)···O(2)	0·958 (1)	3·034 (2)	2·32 (2)
			3·033 (3)	2·216 (3)*
			3·034 (2)	2·217 (2)

$H_2O(3)$		$H_2O(4)$	
H(1)–O(3)–H(2)	109 (1)	H(3)–O(4)–H(3)	112 (2)
	105·69 (12)*		106·42 (20)
	106·05 (11)		106·37 (18)
O(3)–H(1)···O(2)	166 (1)	O(4)–H(1)···O(1)	156 (1)
	162·96 (8)*		158·36 (11)*
	162·86 (10)		158·47 (11)
O(3)–H(2)···O(4)	170 (1)	O(4)–H(3)···O(3)	148 (1)
	178·17 (8)*		142·47 (11)*
	178·02 (9)		142·57 (11)
Li–O(3)–Li	92·15 (8)	O(3)···O(4)···O(3)	87·21 (7)
	92·10 (9)		87·05 (10)
	91·96 (8)		86·96 (7)
Li–O(3)···O(2)	124·09 (4)		
	124·11 (5)		
	124·07 (4)		
Li–O(3)···O(4)	112·22 (4)		
	112·16 (6)		
	112·19 (4)		
O(2)···O(3)···O(4)	93·06 (7)		
	93·17 (8)		
	93·35 (7)		

* Hydrogen positions fixed at neutron values.

A refinement of model *A* at 295 K involving different deformation parameters for all nine atoms did not converge. The number of refined parameters was limited by using a model with only five deformation types. The deformations on O(1) and O(2) and on O(3) and O(4) were each constrained to be equal, and have *mm* site symmetry. Moreover, the deformation was assumed to be the same for all three H atoms. This model led to a significantly lower $wR(F^2)$ value than the spherical-atom refinement. It was unsuccessful, however, in shifting the atoms towards the neutron-determined positions. In fact, the positions for O(3) and O(4) derived from the model *A* deformation refinement differ by as much as 0·018 and 0·020 Å from the more reliable neutron values.

Refinement of *model B* resulted in slightly poorer agreement than for model *A* for both data sets. Large correlation in the model *A* refinements (manifesting itself in large standard deviations of the individual deformation parameters) means that the model *A* deformation density is subject to considerable uncertainty, however. The analysis of the deformation density in $LiNO_3.3H_2O$ is therefore based on maps obtained from model *B*.

Discussion. *Interatomic distances and angles* resulting from *the 120 K X-ray data set* (conventional refinement and deformation refinement, model *A*) are compared with the corresponding neutron values in Table 3. All three sets of non-hydrogen distances [except N–O(2)] agree to within $2\sigma_{\text{combined}}$. The positions from the spherical-atom refinement differ by less than 0·007 (1) Å from the neutron diffraction values, with the shifts occurring towards the lone-pair regions for all O atoms. For both the high-order and the deformation refinements, all atomic positions deviate by $\leq 0{\cdot}005$ (2) Å from the neutron values.

Positions derived from the conventional X-ray refinement differ from the neutron values by less than 0·009 (1) Å *at 295 K*, with the high-order refinement causing small shifts towards the neutron-determined positions. Deviations from the neutron positions after the deformation refinement (model *A*) are as large as 0·018 (5) and 0·020 (5) Å for the O(3) and O(4) atoms, respectively. Distances generally agree within $2\sigma_{\text{combined}}$ for different refinements but in a few cases significant differences arise [Li–O(3): X-ray 2·082 (1) and neutron 2·088 (1) Å; N–O(2): X-ray 1·262 (2) and neutron 1·252 (1) Å].

The general features of the *thermal ellipsoids* for the four experiments are very similar. However, the average ratios *at 295 K* of the mean-square amplitudes of vibration for non-hydrogen atoms, $\langle U_{ii}^{XD}/U_{ii}^{ND} \rangle$, are 1·07, 1·06 and 1·08 ($i = 1, 2, 3$, respectively) (conventional spherical-atom refinement) and 1·00, 1·02 and 1·03 (deformation refinement, model *A*).

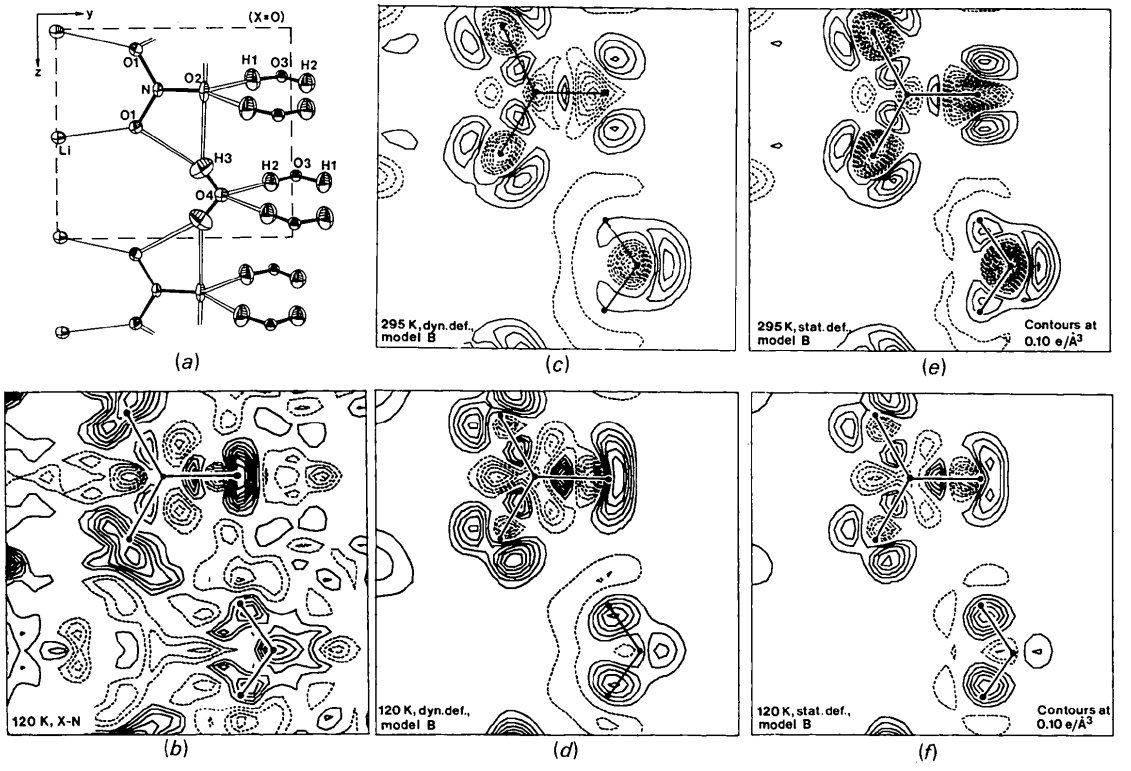

Fig. 1. (*a*) Bonding situations around NO_3^- and $H_2O(4)$. The section displayed in Figs. 1 and 2 is indicated by dashed lines and coincides with the mirror plane through NO_3^-, $H_2O(4)$ and Li^+. The model maps refer to model *B*. The contour interval is 0·05 e Å^{-3} in all maps except Figs. 1(*e*), 1(*f*), 4(*d*) and 4(*e*). Negative contours are dashed and the zero contour is omitted. (*b*) *X*—*N* density at 120 K. (*c*) Dynamic multipole model density at 295 K. (*d*) Dynamic multipole model density at 120 K. (*e*) Static multipole model density at 295 K. (*f*) Static multipole model density at 120 K.

For *the 120 K X-ray data,* the $\langle U_{ii}^{XD}$(high-order)/U_{ii}^{XD}(conventional)$\rangle$ and $\langle U_{ii}^{XD}$(deformation refinement, model *A*)/U_{ii}^{XD}(conventional)$\rangle$ ratios are all between 0·99 and 1·01. The higher $\sin\theta/\lambda$ limit for 120 K data would seem to facilitate a more efficient deconvolution of thermal and valence effects.

There are, however, significant differences between the X-ray and neutron parameters at 120 K. The $\langle U_{ii}^{XD}/U_{ii}^{ND}\rangle$ ratios for the 120 K data are 1·15, 1·11 and 1·12. All U_{ii}^{ND} values were multiplied by a factor 1·13 in an attempt to correct for this effect, which might partly be due to a temperature discrepancy between the neutron and the X-ray experiments, resulting from the temperature fluctuations due to the angle dependence of the temperature attained in the X-ray gas-flow system. The use of such a scaling procedure, although now often accepted practice, can hardly be regarded as satisfactory.

Deformation density maps. In all maps (Figs. 1–5) the reference state is a superposition of the free spherical or spherically averaged electron densities for H, Li^+, N and O. These maps were calculated as Fourier summations over all calculated structure factors (with only the contributions from the deformation functions included) out to the experimental $\sin\theta/\lambda$ limits.

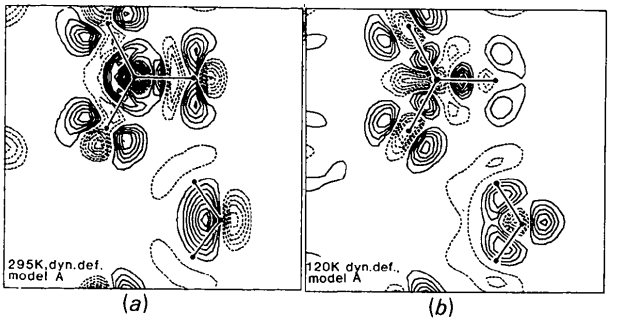

Fig. 2. (*a*) Dynamic multipole model density at 295 K, model *A*. (*b*) Dynamic multipole model density at 120 K, model *A*.

The 295 K *model A* deformation map shows large errors, especially around the water O atoms, reflecting the failure of the refinement of the deformation model. The electron excess in the non-bonding region of the water O atoms has, in fact, been described by a shift of the O nuclei rather than by the deformation functions. The resulting model maps (*e.g.* Fig. 2*a*) actually display electron deficiency in the lone-pair region of O(4).

At 120 K, the deformation refinement model *A* results in atomic parameters rather similar to the neutron parameters. Consequently, the deformation maps from model *A* (Fig. 2*b*) and model *B* (Fig. 1*d*) generally agree [the largest differences occur for the lone-pair regions of O(2) and O(4)].

We have elected to base the discussion of the chemical features in the deformation electron density on maps derived from the refinement of model *B*. The dynamic deformation density derived in such a way is essentially the *X–N* density modelled with multipolar deformation functions. The maps contain no additional information, but have the noise of the *X–N* maps filtered out.

The NO_3^- *ion.* The qualitative features of the deformation density of the NO_3^- ion are quite similar at the two temperatures (Fig. 1*c–f*). There is electron excess in the N–O bonds: maxima of 0·20–0·40 e Å^{-3} for the *static* density and approximately 0·20 and 0·10 e Å^{-3} for the *dynamic* density at 120 and 295 K, respectively. The electron density is markedly elongated perpendicular to the molecular plane for both N–O bonds, indicating a contribution of π bonding (see Fig. 3*a, b*). In the nitrate O lone-pair regions, the *static* density shows two maxima of 0·30–0·50 e Å^{-3} in the molecular plane. The two lone-pair peak heights on O(1) differ by about 0·10 e Å^{-3}. This asymmetry could partly be due to differences in the crystal environment; O(1) has an Li–O contact of 2·18 Å in one direction and accepts a hydrogen bond with an H(3)···O distance of 2·16 Å from the other direction [H(3) forms a weak, bifurcated bond to both O(1) and O(2)]. The lone-pair density is *less* developed in the direction of the presumably stronger Li–O interaction.

The deformation densities associated with several N–O bonds have been studied both experimentally and theoretically. Brief reviews are given by Moss, Guru Row & Coppens (1980) and Hermansson & Thomas (1983).

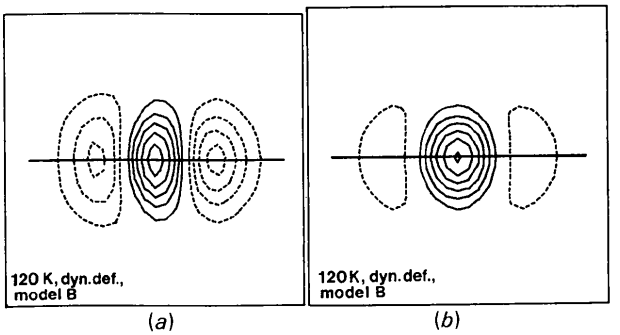

Fig. 3. Dynamic multipole model density at 120 K (model *B*) viewed along the N–O bond direction. The plane of NO_3^- is indicated. (*a*) Through the N–O(1) peak maximum. (*b*) Through the N–O(2) peak maximum.

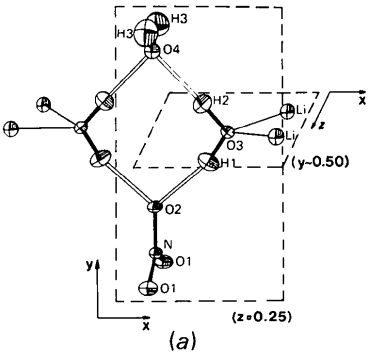

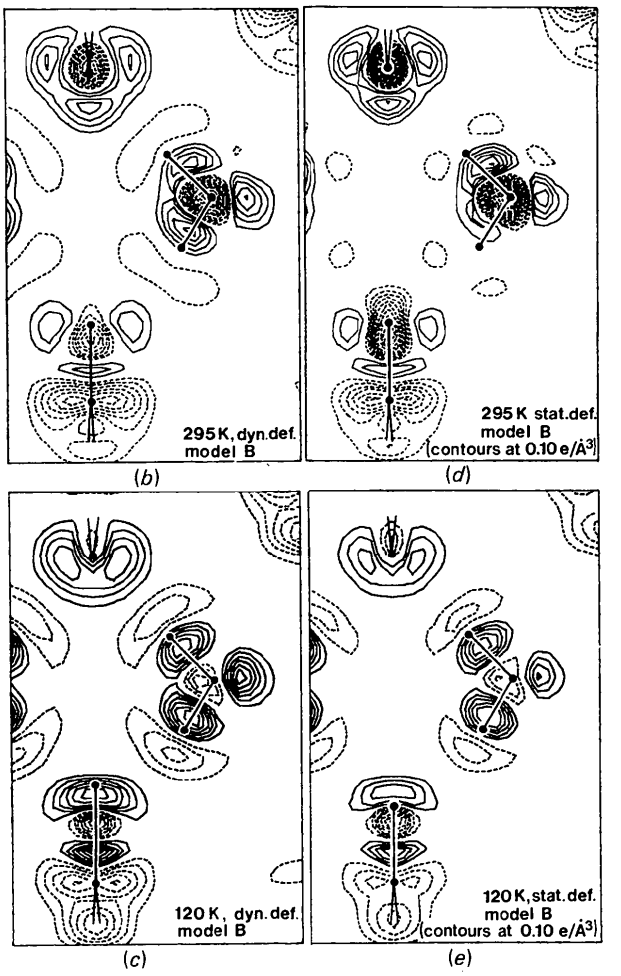

Fig. 4. (*a*) Bonding situation around the $H_2O(3)$ molecule and in the lone-pair plane of the $H_2O(4)$ molecule. The section displayed in Fig. 4(*b–e*) is indicated by the large rectangle and coincides with the mirror plane through O(4), $H_2O(3)$, N and O(2). The small dashed rectangle indicates the section through Li^+–O(3)–Li^+ which is displayed in Fig. 5. The model maps refer to model *B*. (*b*) Dynamic multipole model density at 295 K. (*c*) Dynamic multipole model density at 120 K. (*d*) Static multipole model density at 295 K. (*e*) Static multipole model density at 120 K.

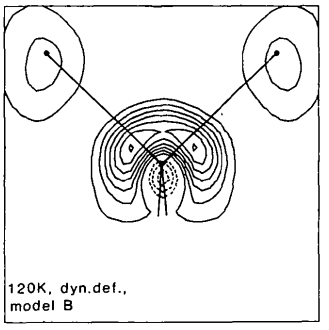

Fig. 5. Section through Li^+—O(3)—Li^+ (see Fig. 4*a*). Dynamic multipole model density at 120 K, model *B*.

The H_2O *molecules and the hydrogen bonds.* The deformation density of the H_2O molecules at 120 K (Figs. 1*d* and 4*c*) shows well developed peaks in the O—H bonds and the O lone-pair regions. There are regions of electron deficiency on the weakly bonded side of the H atoms. The general character of the deformation density in the hydrogen bonds is consistent with what is usually observed for medium-strong and weak O—H···O hydrogen bonds.

A comparison of the deformation densities for the two water molecules shows that the dynamic bond and lone-pair peak maxima for the $H_2O(4)$ molecule are approximately 0·10 e $Å^{-3}$ weaker than for $H_2O(3)$. This is because the thermal parameters of O(4) are approximately 40% larger than those of O(3). For the static density, the O—H bond maxima are all ~0·50 e $Å^{-3}$, and the lone-pair maxima are 0·35 and 0·45 e $Å^{-3}$ for $H_2O(3)$ and $H_2O(4)$, respectively.

The dynamic deformation density for $H_2O(3)$ shows qualitatively the same features at the two temperatures even though, as expected, peak heights are lower and troughs shallower at 295 K. A comparison of the static densities suggests, however, that the 295 K maps suffer from the difficulty in separating the effects of static deformation and thermal smearing. The situation is worse for the $H_2O(4)$ molecule, however. It can be seen directly from the *X—N* map and from Fig. 1(*c*) that the deformation density associated with the O—H bond is almost zero, and that the lone-pair density on O(4) seems exaggerated.

Concluding remarks. The literature to date contains thermally smeared deformation density maps determined at *several temperatures* for some fifteen compounds. Quantitative agreement between the room- and low-temperature densities, although at times satisfactory, is completely absent from a few studies. Comparisons between (presumably) *static* deformation maps at different temperatures have, to our knowledge, only been published for one compound: imidazole at 103 and 293 K (Epstein, Ruble & Craven, 1982). In this case, the general features of the static charge distributions were in good agreement, although some of the C—C bond densities differed by up to 0·50 e $Å^{-3}$.

In both imidazole and $LiNO_3.3H_2O$, the major source of error causing the discrepancies between the static maps is to be found in the refinement of the room-temperature data. The problem would seem to be one of inherently insufficient accuracy in the data. Although *R* values and σ's for positional parameters appear satisfactory, counting statistics are inadequate for an electron density analysis and a proper separation between vibrational and deformation effects. In view of the low melting point of $LiNO_3.3H_2O$(303·1 K) and the consequent large atomic vibrational amplitudes at room temperature [the isotropic r.m.s. amplitude of vibration at 295 K is 0·168 Å for O(3) and 0·200 Å for O(4)], low-temperature data thus seem to be essential for an electron density study of this type of system.

This work has been supported by grants from the Swedish Natural Science Research Council.

References

ABRAHAMS, S. C. & KEVE, E. T. (1974). *Acta Cryst.* A**30**, 580–584.

BECKER, P. & COPPENS, P. (1974). *Acta Cryst.* A**30**, 129–147.

EPSTEIN, J., RUBLE, J. R. & CRAVEN, B. M. (1982). *Acta Cryst.* B**38**, 140–149.

HERMANSSON, K. & THOMAS, J. O. (1983). *Acta Cryst.* C**39**, 930–936.

HERMANSSON, K., THOMAS, J. O. & OLOVSSON, I. (1977). *Acta Cryst.* B**33**, 2857–2861.

HERMANSSON, K., THOMAS, J. O. & OLOVSSON, I. (1980). *Acta Cryst.* B**36**, 1032–1040.

HIRSHFELD, F. L. (1971). *Acta Cryst.* B**27**, 769–781.

International Tables for X-ray Crystallography (1974). Vol. IV, pp. 72–73, 149. Birmingham: Kynoch Press.

LEHMANN, M. S. & LARSEN, F. K. (1974). *Acta Cryst.* A**30**, 580–584.

LUNDGREN, J.-O. (1982) *Crystallographic Computer Programs.* Report UUIC-B13-4-05. Institute of Chemistry, Univ. of Uppsala.

MOSS, G., GURU ROW, T. N. & COPPENS, P. (1980). *Inorg. Chem.* **19**, 2396–2403.

STEVENS, E. D. & COPPENS, P. (1976). *Acta Cryst.* A**32**, 915–917.